Yuan Shi, Fiona Kessel, Martin Friess, Neraj Jain, Kamen Tushtev

Characterization and modeling of tensile properties of continuous fiber reinforced C/C-SiC composite at high temperatures

Journal Article as: peer-reviewed accepted version (Postprint)

DOI of this document*(secondary publication): 10.26092/elib/2616

Publication date of this document: 25/10/2023

* for better findability or for reliable citation

Recommended Citation (primary publication/Version of Record) incl. DOI:

Yuan Shi, Fiona Kessel, Martin Friess, Neraj Jain, Kamen Tushtev,
Characterization and modeling of tensile properties of continuous fiber reinforced C/C-SiC composite at high temperatures,
Journal of the European Ceramic Society, Volume 41, Issue 5, 2021, Pages 3061-3071, ISSN 0955-2219,
https://doi.org/10.1016/j.jeurceramsoc.2020.09.043

Original Article

Characterization and modeling of tensile properties of continuous fiber reinforced C/C-SiC composite at high temperatures

Yuan Shi [a,*], Fiona Kessel [a], Martin Friess [a], Neraj Jain [a], Kamen Tushtev [b]

[a] Institute of Structures and Design, German Aerospace Center Stuttgart, Pfaffenwaldring 38-40, 70569 Stuttgart, Germany
[b] Advanced Ceramics, University of Bremen, Am Biologischen Garten 2, 28359 Bremen, Germany

ARTICLE INFO

Keywords:
C/C-SiC
Mechanical properties
High temperature
Hysteresis measurement
Liquid silicon infiltration (LSI)

ABSTRACT

In order to study the effects of temperature on the material behavior of Liquid Silicon Infiltration (LSI) based continuous carbon fiber reinforced silicon carbide (C/C-SiC), the mechanical properties at room temperature (RT) in in-plane and out-of-plane directions are summarized and the tensile properties of C/C-SiC were then determined at high temperature (HT) 1200 C and 1400 C under quasi static and compliance loading. The stress-strain response of both HT tests is similar and almost no permanent strain can be observed compared to the RT, which can be explained through the relaxation of residual thermal stresses and the crack distribution under various states. The different fracture mechanisms are confirmed by the analysis of fracture surface. Furthermore, based on the analysis of hysteresis measurements at RT, a modeling approach for the prediction of material behavior at HT has been developed and a good agreement between test and modeling results can be observed.

1. Introduction and objective

Thanks to their excellent material properties at high temperature, favorable damage tolerance, and comparatively low density, material development researchers have paid particularly high attention of Ceramic Matrix Composites (CMCs) in recent years. Continuous carbon fiber reinforced carbon silicon carbide (C/C-SiC) produced via Liquid Silicon Infiltration (LSI) process has been successfully used in aerospace, traffic and energy technology since in an inert environment the carbon fibers can tackle application temperatures exceeding 1600 C such as in rocket motors or re-entry conditions from space to earth [1 8]. However, the lack of study of its detailed temperature-dependent mechanical behavior and failure mechanism, especially at high temperatures, limits the commercial exploitation of its potential and further use in new application areas.

The mechanical properties of CMCs are determined by the microstructure of the materials, which in turn might be affected by temperature. In the case of oxide ceramic matrix composites (O-CMC), since the dwelling time by sintering at 1200 C and ageing by thermal treatment at 1100 C for several hours had no influence on the mechanical behavior of the prepreg based O-CMC plates [9], tensile strength and stiffness of Nextel 610 fiber reinforced O-CMCs decreased at 1000 C and 1200 C because of the degradation of fiber properties beyond 1000 C [10]. By comparison, according to some recent studies, the internal residual stress and interface bonding might play an important role in the relationship between temperature and mechanical properties for the Chemical Vapour Infiltration (CVI) based CMCs. For the SiBC modified C/SiC composites, interface bonding strength and elastic modulus increase at HT due to the release of residual thermal stress (RTS) [11]. The tensile behavior of coated C/SiC was influenced by RTS, so that the Young s modulus and strength increase continuously with increasing temperature till approx. 1000 C [12]. Similar phenomenon and results have been reported and discussed in references [13 15]. With the further increase of temperature up to 1800 C or 2300 C, since the Young s modulus increases up to 1000 C and then decreases, the strength fluctuated till the fracture [16,17].

The first experiment of liquid silicon infiltration to porous C/C composites was carried out in the early 1970s [18]. The investigation of liquid siliconization in German Aerospace Center Stuttgart began in the late 1980s. Three-step process for the manufacturing of C/C-SiC material was successfully developed [19]. In the first step, starting with a highly carbonaceous, but costly precursor XP-60, a dense carbon fiber reinforced polymer (CFRP) is achieved using resin transfer moulding (RTM) technique. After that, the CFRP is pyrolyzed at HT to obtain a porous C/C composite with a distinct crack pattern. In the last step, the porous C/C composite was infiltrated with liquid silicon whereby the silicon

* Corresponding author.
E-mail address: yuan.shi@dlr.de (Y. Shi).

reacts with carbon to form dense SiC. The dense carbon fiber bundles are load-bearing as well as providing damage tolerance and are surrounded by a protecting SiC-matrix helping to enhance both the oxidation stability and the wear resistance.

Although the LSI-process is a fast and cost-effective process compared to other CMC manufacturing processes e.g. polymer infiltration and pyrolysis (PIP) and chemical vapour infiltration (CVI), the manufacturing of C/C-SiC was strongly limited to RTM-processing in the early days. In order to have a more versatile process, such as autoclave processing and warm pressing technique, as well as cheap carbon source phenolic resins, were heavily investigated and finally tested successfully in the last decade. One of the most important efforts was the investigation and optimization of special process parameters during curing and pyrolysis with substantial amounts of condensation reactions. This successful development reveals that many process parameters are important for the further improvement of material with enhanced properties on the one hand, and realization of a stable process for series production on the other hand [20]. Therefore, this material is subject to the apparent study and some properties were characterized at room temperature. The ratio of bending to tensile strength of C/C-SiC was about 1.7–2 depending on different loading directions relative to the 0/90° woven carbon fibers [21]. The stress-dependent damage mechanisms of C/C–SiC with different fiber architectures were investigated through modal acoustic emission (AE) technique and a significant damage-related increase in AE energy was observed close to the tensile strength [22]. The influence of coupons numbers on the mechanical properties at RT was identified and different statistical distribution of strength values were found to be resultant of various failure mechanisms [23]. Nevertheless, the effect of temperature, especially close to the max manufacturing temperature, on the mechanical behavior and the associated fracture mechanisms have hitherto not been investigated in detail yet. Therefore, the main objective of this paper is to determine the effect of temperature on the mechanical properties of LSI based C/C-SiC material. Investigations at RT and HT are carried out under quasi-static and compliance tensile loadings. The change of RTS and distribution of cracks under various states are discussed.

Furthermore, based on the works of Evans et al., [24,25] the residual stress of SiC fiber reinforced composite were measured by interrogation of intersection point of unloading–reloading cycles [26,27]. Deng et al. have modelled the effect of RTS over the high temperature strength of C/SiC material based on theoretical models but the underlying phenomenon behind the relationship between the strength at room temperature and high temperature was not studied [28]. Moreover, the model relies on temperature dependent properties like Young's Modulus, release coefficient of RTS, etc. for individual constituents of the composite. A model based on energy balance approach is presented by Li [29], where constituent properties like elastic properties, fibre volume content and fibre/matrix interface properties are used in order to evaluate the temperature dependent proportional limit stress of SiC/SiC. Although these properties might be available for single constituent matrix system (SiC) in the literature but are difficult to evaluate for a relatively complicated multiphase matrix system like C-SiC, which consists of three different chemical phases: C, Si and SiC. As far as the fibre/matrix interface properties of C/C are concerned, the precursor used to form the carbon matrix in an intermediate step plays a major role in the interface strength [30,31]. These fibre/matrix interface properties, in turn, decide the failure behavior of the material but are poorly reported in the literature. The lack of temperature dependent constituent data makes it difficult to evaluate high temperature properties of C/C-SiC. On contrary to the above mentioned models, the proposed model uses an analytical approach based on the hysteresis measurements at RT for the prediction of material behavior of C/C-SiC at HT.

2. Experimental

2.1. Material C/C-SiC

The investigated material C/C-SiC is a continuous fiber reinforced ceramic composite with carbon and silicon carbide matrix, derived from a well standardized woven preform and a pre-infiltration process (prepreg). Bases are 3 K HTA fibers of Teijin Carbon Europe GmbH, woven to a 2/2 twill and a phenolic resin as precursor. The phenolic resin is rich in carbon (~60 mass %) and provides a dimensionally stable structure even after pyrolytic processes. Green plates with dimension 300*300 mm^2 were produced by stacking of several number of woven carbon fabric pre-infiltrated with phenolic resin. In order to get a symmetrical structure, each single layer was rotated by 90° during the ply stacking. Then, C/C-SiC plate was manufactured via Liquid Silicon Infiltration (LSI) process. The LSI process is a relatively low-cost production method for CMC manufacturing with reliable production results. The manufacture process can be summarized in three steps: greenbody shaping, pyrolysis and siliconization [32]. The consolidation took place in an autoclave under max pressure of 20 bar and at 190 °C. Then, the sample was pyrolyzed under inert gas atmosphere (nitrogen) and at max temperature of 1650 °C. During pyrolysis, volatile components from the phenolic matrix evaporate away and results in an amorphous and porous carbon matrix. This process is accompanied by approx. 10 % shrinkage of the material in the thickness direction caused by the mass loses. The carbon fibers are densely packed and embedded in the carbon matrix and a crack pattern (so called "block structure") evolves in a C/C body, which is essential for silicon melt infiltration and prevents the reaction of the utmost carbon fibers in C/C block with liquid silicon. Finally, during the siliconization step silicon with a purity of 99.9 % is melted at temperatures above 1420 °C (max temperature of siliconization step is 1650 °C for approx. 60 min) and liquid silicon infiltrates via capillary forces into the porous carbon body. The crack pattern is filled with silicon which reacts with the carbon (matrix and fiber) to given silicon carbide. Due to the lower density of the carbon matrix, its conversion to silicon carbide is stronger keeping most of the carbon fibers intact. As mentioned in the Section 1, the standard parameters of this manufacturing process had been established in the last decade and the finished C/C-SiC material is shown in Fig. 1. The directions x- and y-axis represent the fiber reinforcement orientation 0° and 90°, respectively, and the z-axis is the out-of-plane direction.

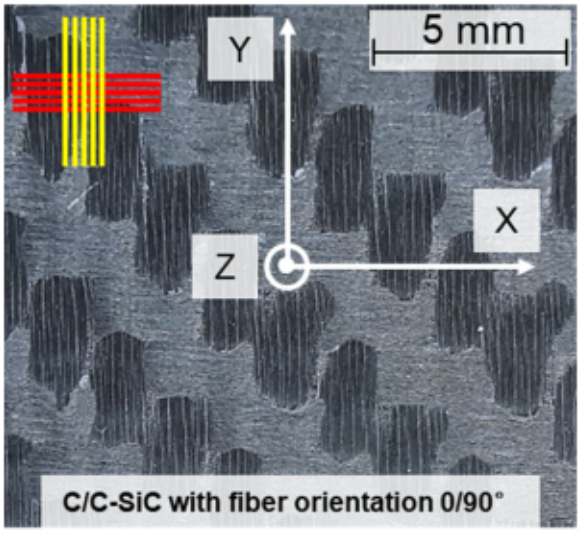

Fig. 1. C/C-SiC plate with fiber orientation of 0/90° and coordinate system in accordance with the mechanical loading directions.

2.2. Material characterisation

The microstructure of samples at different process steps was analyzed by scanning electron microscopy (SEM, Gemini ultra plus from Zeiss Group). For the analysis of the microstructure, small samples were cut from the composite plate and embedded in a conductive resin. For the microstructure images, an AsB detector (Angle selective Backscatter) was used and the phase composition was analyzed with the open source software ImageJ (Version ImageJ 1.52p, Java 1.8.0_172, 64-bit).

Phase analysis was performed by X-ray diffraction (XRD) using a 2θ-goniometer (D8 Advance, Bruker AXS, Germany) with Cu K_α radiation (154.060 pm) with a step size of 0.02° and 10 s time/step in the range of $10° < 2\theta < 90°$.

The fiber volume content of C/C-SiC was calculated by the measurement of the initial weight of the carbon fibers and the total volume of the finished component. The density and porosity of the manufactured plate material were measured using the Archimedes method [33]. It was carried out on the component before sample cutting.

The coefficient of thermal expansion (CTE) of C/C-SiC was measured via dilatometry (Netzsch GmbH) according to DIN EN 1159-1:2003. The samples were prepared in two different orientations: in x - or y - direction to determine the in-plane CTE value; in z – direction for the out-of-plane value. The dimension of in-plane samples is $4 \times 5 \times 25$ mm^3 and due to the limit of the plate thickness the length of the out-of-plane sample is 15 mm. Five samples of each orientation were tested. Testing conditions were under inert atmosphere (argon) and a start temperature of 25 °C up to a max. of 1300 °C. The heating rate was kept constant at 5 K/min.

The specific heat capacity (C_p) and thermal conductivity (λ) were measured between room temperature (25 °C) and 1000 °C with laser flash analyses (LFA) method [34] with a LFA 457 (Netzsch GmbH). The sample dimensions are 12.6 mm in diameter and height of 2.5 mm. For

Table 1
Specimen geometry with dimensions, loading direction for different mechanical tests at RT, in-plane tensile test at HT and the associated DIN EN standards.

Test	Standard	Specimen geometries, dimensions and loading direction
In-plane tensile with t_x of 5 mm (Quasi static and cyclic loading-unloading at RT)	DIN EN 658-1: 1999	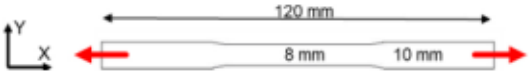
Out-of-plane tensile with t_y of 20 mm	–	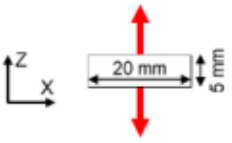
In-plane compression with t_x of 5 mm	DIN EN 658-2: 2003	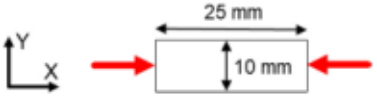
Out-of-plane compression with t_y of 5 mm	–	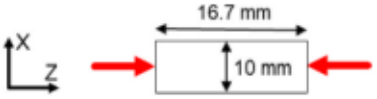
In-plane shear (Iosipescu) with t_x of 3 mm	DIN EN 12289: 2005	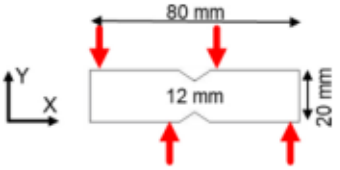
Out-of-plane shear (Iosipescu) with t_y of 3 mm	–	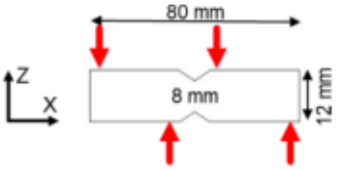
In-plane 3PB with t_y of 10 mm	DIN EN 658-3: 2002	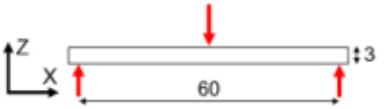
Interlaminar shear of notched samples with t_y of 10 mm	DIN EN 658-4: 2003	
In-plane tensile at HT with t_x of 4 mm	DIN EN 1892:2005	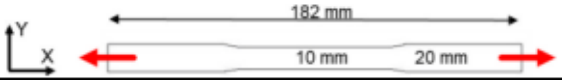

statistical confirmation at least three samples per specimen orientation were tested.

For a better understanding of material behavior, the RT mechanical properties of the investigated C/C-SiC material with fiber orientation 0/90 , including Young s modulus, strength and fracture strain, were completely evaluated with in-plane and out-of-plane experimental tests. The samples for the experiments were cut from flat plates with different thicknesses. Table 1 gives an overview of the performed mechanical tests with the associated DIN EN standards, specimen size and the loading direction relative to the specimen geometries, where t_n (n y *or* z) is the thickness of specimen, which is not shown in the schematic images. The axis x and y represent the fiber directions (see Fig. 1). To the best knowledge of the authors, there are no available DIN or EN standards for the tensile, compression and shear tests in out-of-plane direction. Therefore, these three tests were conducted and evaluated according to the internal developed procedures at the institute. For the out-of-plane tension test, the both surface areas (x y plane) of C/C-SiC sample were bonded to 2 metal adapters with epoxy adhesive. After the hardening of adhesive, the adapters were clamped by the normal grip system of testing machine.

The experiments were performed in air under quasi-static loading and up to failure of sample on a universal testing machine (Zwick 1494) at a controlled cross head speed of 1 mm/min. The failure stress was calculated from the maximum load and the initial cross-section of the samples. For statistical confirmation at least five samples per series were tested. In-plane tensile specimens with the dimensions of 120*10(8)*5 mm^3 (Table 1) were produced with a reduced cross section in their gauge areas. For the tensile and compression tests, the longitudinal and the transverse strains relative to the loading direction were measured with strain gauges. During shear tests, the strains were evaluated using strain gauges in the 45 and in the -45 directions relative to the shear loading direction and the strain gauges were glued on both sides of the sample in the area between the notches. The bending properties of the C/C-SiC materials were determined by three-point-bending (3PB) test according to DIN-EN 658-3 with a span-to thickness ratio of 20. The longitudinal strains were measured with strain gauges on the tensile site of bending specimens. In order to determine the interlaminar shear strength, compression-shear test was performed according to DIN-EN 658-4 with a notch distance of 8 mm.

2.3. Compliance tensile test at RT

In this work, identical in-plane tensile specimen (Table 1 first row) was employed to do the cyclic loading-unloading test (compliance test) with a loading rate of 1 mm/min at RT. Similar to quasi static tests, strain gauges were glued on the opposite sides of each specimen to monitor the strains. The first cycle of loading-unloading was at 30 MPa and unloaded at the same crosshead speed to near zero force, then an incremental step loading of 20 MPa per cycle up to final rupture of specimen was carried out. Three samples at RT were investigated.

2.4. Tensile test at HT

In order to determine the influence of high temperature on the mechanical properties of the C/C-SiC material, in-plane tensile specimens with the shape in Table 1 (last row) were investigated at HT in argon. In order to avoid the melting of residual silicon in C/C-SiC, the test temperature should be set at a lower temperature than the melting point of Si (about 1420 C). On the other hand, for the test setup used in this work, it is still possible to record relatively good stress-strain curves at the max temperature of 1400 C and due to the fact that the mechanical test at HT is very complex and time-consuming, especially cyclic loading-unloading test, one sample was loaded quasi-static and two others were tested with loading-unloading cycles (compliance test) as defined for the RT tensile tests (Section 2.3) for 1400 C. Furthermore, according to the authors own knowledge and experience, 1200 C is a typical application temperature of C/C-SiC in aerospace and civil engineering field, five samples were tested at 1200 C under quasi-static loading until ultimate failure. All high temperature tests were performed with a loading rate of 0.5 mm/min on a universal testing machine Zwick/Roell 1465 equipped with a vacuum chamber and an induction unit EMA HG1-DS, EMA Indutec GmbH, Germany. The longitudinal strain at HT was measured using a laser extensometer P-50, Fiedler Optoelektronik, Germany.

3. Results

3.1. Microstructure and phase evolution

SEM pictures of Fig. 2 shows the microstructure of samples at different process steps. The polished samples have a cross section of the plate material with fiber orientation in x -direction horizontal in the image and y -orientation perpendicular to the image-plane. As mentioned before, the x- and y-axis represent the fiber orientation 0 and 90 , respectively. The microstructure of the resulting carbon fiber reinforced polymer body (CFRP) can be seen in Fig. 2a. Filament bundles (rovings) oriented in 0 and 90 and the staking of layers are clearly visible. In addition, the image shows that in the green body state small quantities of porosity and matrix enclosures are always present. The porosity in this state is approx. 1.5 %.

After the pyrolysis process, a crack pattern evolves in the C/C body, as can be seen in Fig. 2b, which is typical for C/C-SiC via LSI process. It has macro cracks inside, which propagate through the structure. Longitudinal or transverse channels result in an open porosity of approx. 20 %. This crack pattern is essential for the resulting material properties, since the block like structure, defines the porosity and channels for liquid silicon penetration during melt infiltration. Apart from the guidance for the melt, the block structure ensures the fiber integrity by restricting the reactive areas only inside the cavities. The fibers inside the blocks are well protected from reaction with the silicon and can provide the desired damage tolerance to the material.

In Fig. 2c the microstructure after the liquid silicon infiltration is shown, when the cavities of the crack pattern are filled with SiC, after the reaction of carbon and silicon. An analysis of the material phase composition via ImageJ (analyzed number of samples is five and the area of each image is 3.5 mm^2) gave a share of the carbon (81 86 vol. % carbon fibers and amorphous carbon matrix), silicon carbide (11 15 vol. %) and residual silicon (1 4 vol. %) distribution.

Phase evolution of C/C-SiC was performed by XRD measurement as shown in Fig. 3. Only -SiC, C and residual Si from the liquid silicon infiltration process can be detected and no formation of -SiC was observed. It should be noted that the carbon peaks are due to the carbon fibers and not to the carbon matrix since the same X-ray analysis of previous work for SiC fiber reinforced carbon (SiC/C) or SiC fiber reinforced SiC (SiC/SiC) do not show this carbon peak (to be published).

3.2. Material properties

The fiber volume content, the porosity and the density of the manufactured C/C-SiC material are 60 %, 1.2 % and 2.0 g/cm^3, respectively.

The thermal expansion behavior of C/C-SiC material was measured from room temperature to 1300 C and the length change in in-plane (x- and y-orientation) and out-of-plane (z-orientation) directions was recorded. As shown in Fig. 4, the CTE values in in-plane direction are very low, or even negative below 300 C, while the values in z-orientation (out-of-plane) are considerable higher. The CTE values at RT are -1.50 10 ^{6} K^{-1} in x- and y-orientation, and 5.22 10 ^{6} K^{-1} in z-orientation. Then, the CTE values increased with rising temperature and reached 2.27 10 ^{6} K^{-1} (x- and y-orientation) and 6.05 10 ^{6} K^{-1} (z-orientation) at 1300 C, respectively. The results show that the difference in fiber orientation affects the material properties drastically: the CTE values for x- and y-orientation are mainly influenced by the CTE of fiber (e.g. 1.6

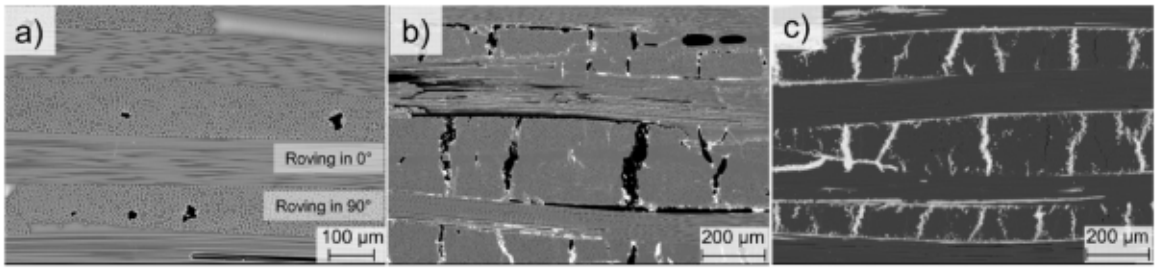

Fig. 2. Microstructure of samples with 0/90° fiber orientation at different process step: a) CFRP state after consolidation; b) C/C state after pyrolysis and c) C/C-SiC after siliconization.

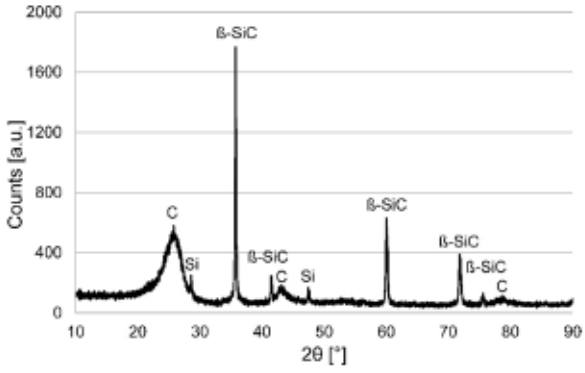

Fig. 3. XRD pattern of C/C-SiC composite.

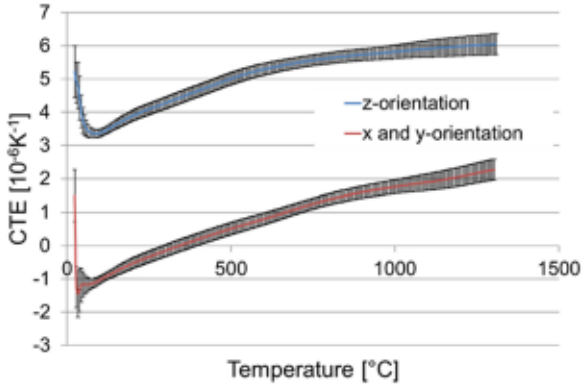

Fig. 4. Relationship between CTE and temperature of C/C-SiC material in x- (y-) and z-directions.

10^{-6} K^{-1} at RT [35]), while the CTE value of the z- orientation are strongly dependent on the CTE of matrix (e.g. 3.5 10^{-6} K^{-1} at RT [36]).

The characterization of the thermal conductivity (λ) and the specific heat capacity (c_p) of C/C-SiC in in-plane and out-of-plane directions were measured from RT to 1000 °C with each step of 100 K via LFA method. The results of λ as shown in Fig. 5a reveals that the heat conduction along the fiber direction (x-/y-orientation) is significantly faster than in the perpendicular direction (z-orientation). Though the c_p value should be theoretically independent on the direction of measurement or fiber orientation for composite material, a slight offset between in-plane (x-/y-orientation) and out-of-plane (z-orientation) directions can be observed in Fig. 5b, which could be explained by the fact that the measurement of c_p was influenced by the different values of λ of C/C-SiC.

The mean value and standard deviation of C/C-SiC material with fiber orientation 0/90° under tensile, compressive and shear load are summarized in Table 2. At first, the determination of the elastic constants was conducted using a linear fit of the initial linear region of the stress-strain curves. E is the Young's modulus, ν is the Poisson's ratio and G the shear modulus. As mentioned before, the indices x, y and z correspond to the indications in Fig. 1 and Table 1. The x- and y-axis represent the fiber orientation 0° and 90°, respectively, and the z-axis is the out-of-plane direction. The index T denotes the tensile test and C the compression test. As mentioned in Section 2.1, the green plates of C/C-SiC were produced by stacking of several layers and each single layer was rotated by 90° during the ply stacking in order to get a symmetrical structure. Due to this symmetry of fiber orientation 0/90° the Young's modulus E_x is equal to E_y, and the values of the Poisson's ratio ν_{xz} and ν_{zy}, shear modulus G_{xz} and G_{zy} are theoretically identical, respectively. The same material properties of C/C-SiC in x- and y-direction were verified through samples, which were prepared and investigated in both in-plane directions in several internal projects. Furthermore, the strength values under different loading directions were calculated from the maximum force using the formulas for the related tests. The determined tensile and compression strengths σ and shear strengths τ are listed in Table 2. For orientation 0°/90° the strength values σ_x and σ_y, τ_{xz} and τ_{zy} are assumed to be identical, respectively. In addition, the fracture strain ε under tensile or compression loading and γ of shear test was defined as the strain value at the related maximum strength, which are listed in Table 2 too. Similar to elastic constants and strength, the ultimate strain ε_x is equal to ε_y, and γ_{xz} equal to γ_{zy}. It should be noted that the mechanical properties under out-of-plane compression loading have been published in the previous work [37]. The elastic constants, strength values and fracture strain obtained from in-plane 3PB and interlaminar shear test are summarized in Table 2. Since the Young's modulus under tensile and flexure loading are comparable, the strength and ultimate strain of 3PB test are significantly higher than the values of tensile test.

3.3. Results of compliance test at RT

The in-plane tensile stress-strain curves (in x or y direction) with loading-unloading cycles of C/C-SiC obtained at RT are shown in Fig. 6. Above a given applied stress, the curves do not superimpose and give rise to the formation of a slight hysteresis loop. The permanent strain increased with growth of cycles. The Young's modulus was evaluated using a linear fit of the initial linear region before the first cycle. The evaluated mechanical properties are summarized in Table 3 and compared with the quasi static results at RT. With consideration of the standard deviation, the values of the quasi static (from Table 2) and the cyclic loading-unloading tests at RT are highly comparable. Therefore, it is reasonable to conclude that cyclic loading-unloading for low number of cycles has almost no influence on the mechanical properties of C/C-SiC.

3.4. Results of tensile test at HT

The typical tensile stress-strain curves under compliance and quasi static loading at 1400 °C, and under quasi static loading at 1200 °C are shown in Fig. 7. In order to present a better comparison with the curves the strain axis is offset with 1‰ and 2‰ for 1400-T and 1200-T, respectively. The stress-strain responses at both temperatures are

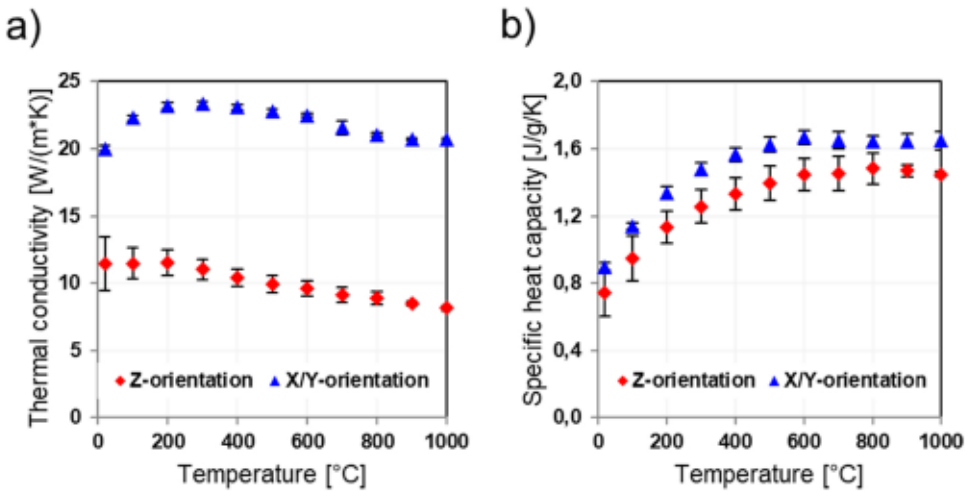

Fig. 5. a) Thermal conductivity and b) specific heat capacity of C/C-SiC material in x- (y-) and z-directions.

Table 2
Summary of elastic constants, strength values and fracture strain of material C/C-SiC (0/90°) in directions x, y and z obtained from tensile, compression, Iosipescu-shear, 3PB and interlaminar shear tests. The index T denotes the tensile test and C the compression test.

Elastic constants in directions x, y and z obtained from tensile and Iosipescu-shear tests					
$E_x^T = E_y^T$ [GPa]	E_z^T [GPa]	ν_{xy}^T [-]	$\nu_{xz}^T = \nu_{xy}^T$ [-]	G_{xy} [GPa]	$G_{xz} = G_{xy}$ [GPa]
72.8 ± 2.1	28.7 ± 0.7	0.02 ± 0.01	0.04 ± 0.01	9.5 ± 1.7	20.3 ± 1.2
Elastic constants in directions x, y and z obtained from compression test					
$E_x^C = E_y^C$ [GPa]	E_z^C [GPa]	ν_{xy}^C [-]	$\nu_{xz}^C = \nu_{xy}^C$ [-]		
84.2 ± 11.6	28.3 ± 1.9	–	0.06 ± 0.01		
Strength values in directions x, y and z obtained from tensile, compression and Iosipescu-shear tests					
$\sigma_x^T = \sigma_y^T$ [MPa]	σ_z^T [MPa]	$\sigma_x^C = \sigma_y^C$ [MPa]	σ_z^C [MPa]	τ_{xy} [MPa]	$\tau_{xz} = \tau_{xy}$ [MPa]
125.7 ± 13.1	11.9 ± 0.5	329.9 ± 15.4	360.8 ± 32.4	71.7 ± 0.9	55.1 ± 6.4
Fracture strain values in directions x, y and z obtained from tensile, compression and Iosipescu-shear tests					
$\epsilon_x^T = \epsilon_y^T$ [%]	ϵ_z^T [%]	$\epsilon_x^C = \epsilon_y^C$ [%]	ϵ_z^C [%]	γ_{xy} [%]	$\gamma_{xz} = \gamma_{xy}$ [%]
0.25 ± 0.03	0.04 ± 0.01	–	1.14 ± 0.16	3.09 ± 0.13	0.95 ± 0.28
Mechanical properties obtained from 3PB test				Interlaminar shear strength	
$E_x^B = E_y^B$ [GPa]	$\sigma_x^B = \sigma_y^B$ [MPa]	$\epsilon_x^B = \epsilon_y^B$ [%]		$\sigma_x^{ILSS} = \sigma_y^{ILSS}$ [MPa]	
69.3 ± 2.2	209.1 ± 13.8	0.41 ± 0.04		24.8 ± 3.8	

similar. In contrast to the behavior with compliance cycles at RT (Fig. 6), the loading and unloading loops at different stresses at 1400 °C almost overlap each other, no significant hysteresis loop and permanent strain can be observed. The evaluated mechanical properties at both temperatures are comparable and summarized in Table 3. In contrast to the results of RT, the Young's modulus is almost constant with increasing test temperature. Despite the large standard deviation, a decreasing tendency of the mean value of the fracture strain can be recognized with increasing temperature (Table 3 and Fig. 10b).

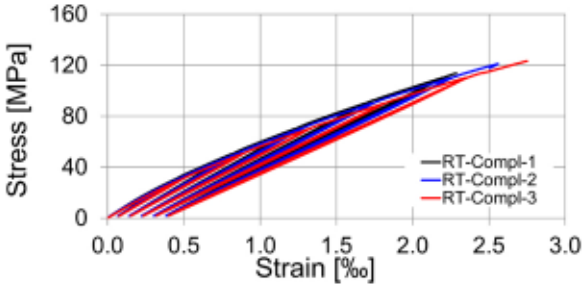

Fig. 6. Stress-strain behaviors of C/C-SiC material under tensile loading-unloading cycles at RT.

Table 3
Mechanical properties of C/C-SiC under tensile loading at RT, 1200 °C and 1400 °C.

Temperature	Loading	$E_x^T = E_y^T$ [GPa]	$\sigma_x^T = \sigma_y^T$ [MPa]	$\epsilon_x^T = \epsilon_y^T$ [%]
RT	Quasi static (from Table 2)	72.8 ± 2.1	125.7 ± 13.1	0.25 ± 0.03
	Cyclic loading-unloading	72.3 ± 4.3	119.2 ± 5.0	0.25 ± 0.02
1200 °C	Quasi static	72.3 ± 15.7	143.1 ± 8.9	0.22 ± 0.02
1400 °C	Quasi static and cyclic loading-unloading	76.2 ± 10.4	137.7 ± 16.8	0.20 ± 0.03

4. Discussion

4.1. Influence of temperature on mechanical properties

As mentioned above, a nonlinear stress-strain behavior with significant permanent strain and change of stiffness can be observed under tensile loading at RT (Fig. 6). Fig. 8 shows the dependence of the stiffness and the permanent strain of each cycle on the loading stress of compliance test. The Young's modulus of 72.2 GPa continuously reduces to the stiffness of approx. 57.5 GPa by the last cycle. In comparison, permanent strain grows proportionally with the number of the loading-unloading cycles i.e. with the incremental increase in loading stress.

On the contrary, the curves of loading-unloading test at 1400 °C (1400-Compl in Fig. 7) almost superimpose on each other without permanent strain and reduction of stiffness during each cycle. As the

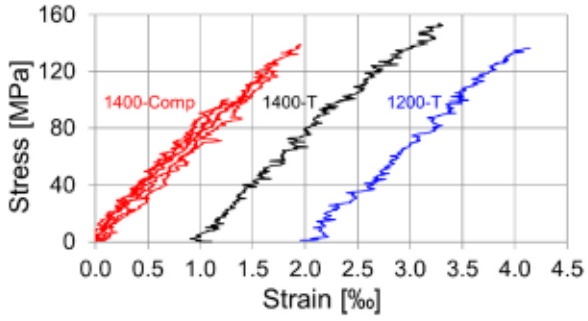

Fig. 7. Tensile stress-strain behaviors of C/C-SiC material under compliance loading at 1400 °C (1400-Comp), under quasi static loading at 1400 °C (1400-T) and under quasi static loading at 1200 °C (1200-T). Offset of strain axis with 1‰ and 2‰ for 1400-T and 1200-T, respectively.

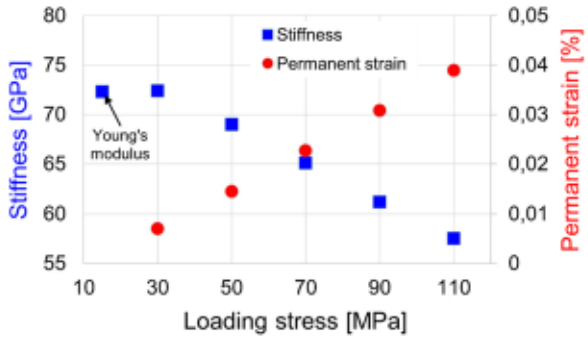

Fig. 8. Effect of the loading stress of compliance test on the stiffness and the permanent strain of each cycle at RT.

temperature range of the HT-investigation is lower than the maximum processing temperature of C/C-SiC (pyrolysis and siliconization at 1650 °C), both the fiber and matrix are refractory and therefore, their mechanical properties are assumed to remain unchanged during the HT tensile test. In this case, the difference in tensile behavior at RT and 1400 °C can be explained exclusively by the residual thermal stresses (RTS) in the fiber and the matrix. Because of the mismatch of coefficient of thermal expansion (CTE) value of carbon fiber and SiC matrix, the RTS generates in C/C-SiC after the last step of HT manufacturing process (siliconization at 1650 °C). Though the CTE value of -0.1 [10^{-6}/K] for HTA 40 carbon fiber in the longitudinal direction can be found in the manufacture datasheet [38], the CTE measurement of pure matrix of C/C-SiC poses a challenge because of its multiphase (C, Si and SiC) matrix system. However, the composition of material MiCaSiC®, which was developed at DLR and manufactured through same LSI process as C/C-SiC, is well comparable to the matrix of C/C-SiC. The CTE value of MiCaSiC® has been measured and is approx. 3.9 [10^{-6}/K] [39], which is significantly higher than the value of fiber. Therefore, the high process temperature and the CTE mismatch between fiber and matrix leads to development of RTS when cooling down the C/C-SiC composite to RT. As a result, tensile stress exists in the matrix and the fiber is under compressive stress at RT. Similar phenomenon has been reported in the case of other CMCs like Ultra High-Temperature CMCs where there is a difference between the CTEs of fiber and matrix [40].

In order to explain the different material behavior of C/C-SiC at RT and HT close to the temperature at the last processing step, a schematic representation for the change of RTS (red arrows) and cracks distribution of C/C-SiC under different tensile loading states and temperature conditions is shown in Fig. 9. As already discussed, tension and compression RTS are present in matrix and fiber of C/C-SiC respectively. Under tensile loading at RT (Fig. 9, left), due to the relatively small tensile force (F_0 to F_1), no matrix crack develops and the Young's modulus can be evaluated in this initial linear region. As the force increases above a given applied stress, cracks will appear and develop

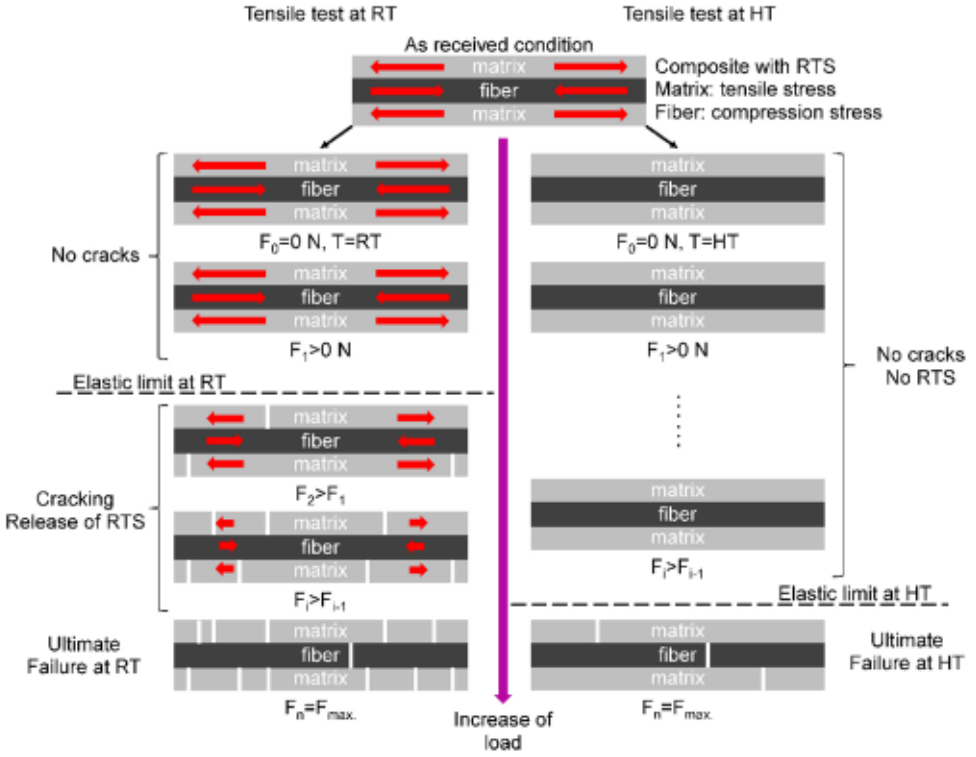

Fig. 9. Schematic representation for the change of residual thermal stresses (RTS red arrows) and crack development-distribution of C/C-SiC under tensile loading at RT and at HT close to the temperature at the last processing step (For interpretation of the references to colour in this figure legend, the reader is referred to the web version of this article).

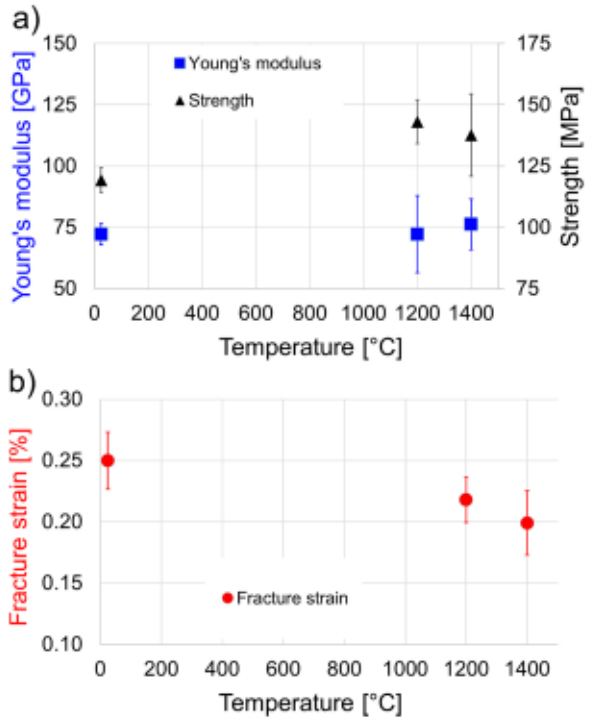

Fig. 10. Dependence of a) the Young's modulus, the strength and b) the fracture strain of C/C-SiC on the test temperature.

throughout the matrix (from F_2 to F_i). Due to the damage of the matrix, a significant degradation of composite's stiffness and increased permanent strain at RT was observed, as shown in Fig. 8. The permanent strain is due to the incomplete crack closure after the unloading.

On the other hand, gradual crack formation in the matrix leads to continuous decrease in RTS. With increase in tensile loading and further crack development, the RTS reduces to zero and once the loading exceeds the failure strain of fiber (F_n), the composite finally ruptures.

Contrarily, in the case of HT test, as shown in Fig. 9 right, RTS from fiber and matrix are released during the HT (close to the manufacturing temperature of C/C-SiC), especially in the test at 1400 °C. As a result, no matrix crack development is observed from F_0 to F_i. Because of this phenomenon, almost no permanent strain could be observed during the tensile loading-unloading test at HT. Compared to the tensile test at RT, the elastic limit at HT, which is related to the onset of cracking of the matrix, is considerably broader because the matrix is not preloaded in tension. Similar to the test at RT, C/C-SiC composite will fail as soon as the failure strain of fiber is achieved.

It should be noticed that determination of the accurate stress value at which cracks begin to appear in the matrix may be feasible through in-situ SEM, computer tomography (CT) or Acoustic Emission (AE) examination at different temperatures, which are very complex and time-consuming. However, in this study the matrix dominated properties of C/C-SiC at RT was investigated under the tensile loading in out-of-plan direction and the strength value is approx. 11.9 MPa (Table 2), and it is reasonable to assume that the stress values of crack initiation in the matrix at RT should be smaller than it. On the other hand, according to the developed modeling approach in this work, the difference in the corresponding stresses and strains at RT and HT can be explained through the relaxation of thermal residual stress and the elastic limit at HT can be extended from the common intersection of the RT compliance slopes to the appearing of matrix cracks at RT (detailed explanation in Section 4.3). In this case, the minimum stress of crack initiation at HT near to the max manufacturing temperature should be lower than 100 MPa.

In this way, the effect of temperature on mechanical properties of C/C-SiC can be explained through different crack development under tensile loading in Fig. 9. Fig. 10 shows the effect of test temperature on the Young's modulus, the strength and the fracture strain of C/C-SiC. The Young's modulus remains constant in the whole range from RT to HT, because the elastic property is evaluated from initial linear region without development of matrix cracks (F_1 in Fig. 9). On the other hand, due to the release of the compressive RTS in the fibers and almost no evolution of permanent strain during the tensile test at HT (1400 °C), the fracture strain decreases with increasing test temperature. Since the test temperature at 1400 °C is close to the temperature of the last step of manufacturing process, the RTS are released to a higher extent compared to the RT and 1200 °C, which leads to the lowest fracture strain in the test temperature range (Fig. 10b). Furthermore, according to the concept shown in Fig. 9, the whole amount of matrix crack at HT should be lesser than the state at RT, which explains the direct proportionality between tensile strength and testing temperature. The inconsistent tendency between both the HT tests can be explained through the relatively high standard deviation of results obtained from the tests at 1400 °C.

4.2. Analysis of fracture surface

In order to confirm the concept of crack development of C/C-SiC under different temperature conditions (Fig. 9), the fracture surface of the failed samples through tensile test at RT and 1400 °C was analyzed by means of SEM. At first sight, no considerable difference can be observed in the fracture surfaces of samples tested at RT and 1400 °C (Fig. 11a and b), as both the images show significant fiber and fiber-bundle pull-out effect. However, enlargement of several positions of RT test samples in Fig. 11c and e indicate large numbers of cracks in matrix area (red arrows). On the contrary, only few matrix cracks can be observed in Fig. 11d and f for the failed sample of tensile test at 1400 °C. These different fracture mechanisms correlate strongly with the change of stiffness and permanent strain at RT in Fig. 8, the concept of crack development and distribution in Fig. 9 and the results of dependence of the mechanical properties on the temperature (Fig. 10).

4.3. Modeling of mechanical behavior at HT

For the modeling of the mechanical properties of C/C-SiC under tensile loading at 1400 °C, which is near the max temperature during the siliconization step, an approach was developed based on the analysis of hysteresis measurements at RT (Fig. 6) and introduced in this section.

From the stress-strain behavior of loading-unloading test, a common intersection point was found [41,42], as shown in Fig. 12, by extrapolation of the compliance slopes of the top linear portion of each hysteresis loop at RT. Due to the fact that the RTS from fiber and matrix were released at HT (Fig. 9), especially at 1400 °C, the common intersection is the origin free with RTS of C/C-SiC. In this way a new coordinate system with the intersection point P_{00} as original point can be defined for the mechanical behavior of C/C-SiC under tensile loading at 1400 °C. The strain (ε_i) and stress (σ_i) value of the top linear portion of each hysteresis loop at RT were recorded and the position of the point P_{00} ($\overline{\sigma_{00}}$ and $\overline{\varepsilon_{00}}$) can be calculated as:

$$\sigma_{00}^{i} - \sigma_i = k_i(\varepsilon_{00}^{i} - \varepsilon_i) \tag{1}$$

$$\overline{\sigma_{00}} = \frac{\sum_1^i \sigma_{00}^{i}}{i} \tag{2}$$

$$\overline{\varepsilon_{00}} = \frac{\sum_1^i \varepsilon_{00}^{i}}{i} \tag{3}$$

where k_i is the slope of each hysteresis loop, $\overline{\sigma_{00}}$ and $\overline{\varepsilon_{00}}$ are the mean value of σ_{00}^{i} and ε_{00}^{i}, which are the position of the intersection point of each loop. According to the Eq. 1 to 3, the value of $\overline{\sigma_{00}}$ and $\overline{\varepsilon_{00}}$ for the

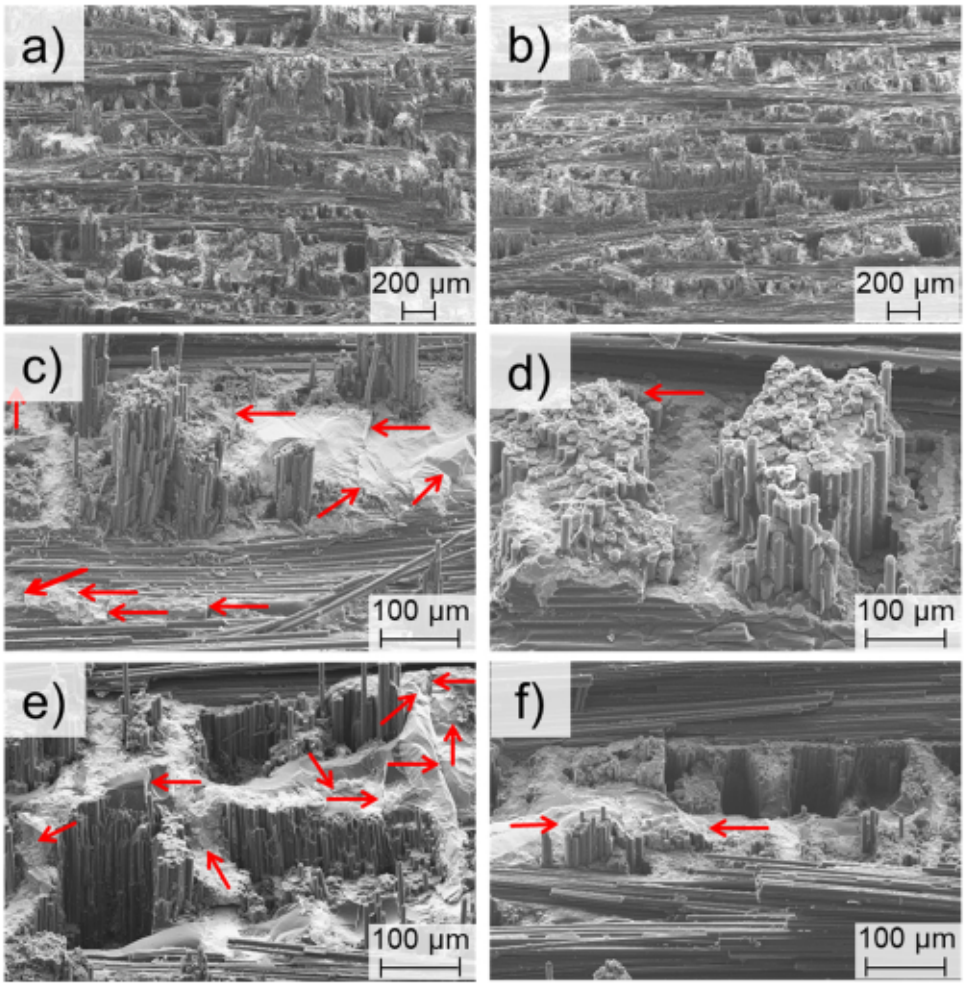

Fig. 11. SEM images for the fracture surface of the samples after tensile test at a), c), e) RT and b), d) f) 1400 °C.

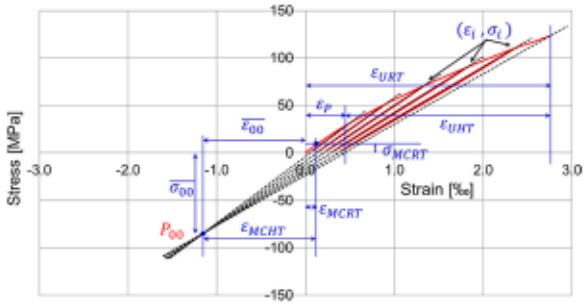

Fig. 12. Common intersection point P_{00} of the C/C-SiC compliance slopes at RT with the associated σ_{00} and ε_{00} to the original coordinate system; ε_i and σ_i are the strain and stress value of the top linear portion of each hysteresis loop. Different values are defined as: ε_{URT}: ultimate strain at RT; ε_{UHT}: ultimate strain at HT; ε_P: permanent strain at RT; ε_{MCRT}: elastic strain value at RT with the associated stress value σ_{MCRT}; ε_{MCHT}: elastic strain value at HT.

point P_{00} has been calculated as approx.−84 MPa and-1.1‰, respectively.

Then, based on the assumption that the temperature range of 1400 °C during the HT-investigation has no influence on the material properties of fiber and matrix, a linear stress-strain relationship from intersection point P_{00} to the strain of matrix cracking at RT is expected and the elastic strain value ε_{MCHT} with the associated stress value (σ_{MCHT}) at HT can be calculated separately as:

$$\varepsilon_{MCHT} = Abs(\overline{\varepsilon_{00}}) + \varepsilon_{MCRT} \quad (4)$$

$$\sigma_{MCHT} = Abs(\overline{\sigma_{00}}) + \sigma_{MCRT} \quad (5)$$

As discussed in Section 4.1, the stress values of crack initiation in the matrix at RT should be smaller than the tensile strength in out-of-plane direction. For the further verification of the modeling approach, the stress value σ_{MCHT} of the elastic range of C/C-SiC was difined as 10 MPa.

Furthermore, the stress-strain curve in Fig. 12 shows accumulation of permanent strain ε_P after unloading until failure of composites at RT. Due to the relaxation of RTS at temperature of 1400 °C, the value of ultimate strain at HT (ε_{UHT}) of C/C-SiC material could be considered as the difference between the ultimate strain at RT (ε_{URT}) and the max permanent strain ε_P at RT:

$$\varepsilon_{UHT} = \varepsilon_{URT} - \varepsilon_P \quad (6)$$

where the ε_P can be identified through the cross point between the strain axis (x-axis) and the line from intersection point P_{00} to ultimate point of stress-strain curve Fig. 12.

By using the modeling approach as explained above, the material properties of C/C-SiC under in-plane tensile loading at 1400 °C are calculated and compared with the experimental results at different temperatures in Fig. 13. Due to the fact that the modeling approach was developed for the prediction of tensile properties at HT close to the max manufacturing temperature of C/C-SiC, a stronger agreement between calculated and test results at 1400 °C can be observed compared to the RT and 1200 °C, especially for the fracture strain.

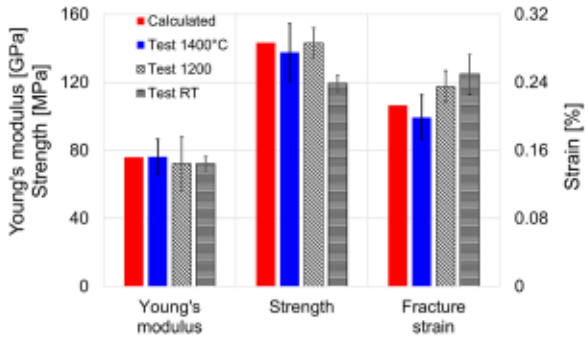

Fig. 13. Comparison of the calculated material properties with the experiment values of C/C-SiC under in-plane tensile loading at RT, 1200 °C and 1400 °C.

It is important to mention that, a point-by-point modeling of material behavior up to its ultimate failure is not the aim of this study. Nevertheless, a bilinear model with the calculated values from Fig. 13 was used to describe the composite behavior at 1400 °C under tensile loading. The stress-strain comparison diagrams with test and calculated results are summarized in Fig. 14 and a very close correlation can be observed. This modeling approach based on the analysis of hysteresis measurements at RT may be applicable for the prediction of the mechanical properties at HT of C/C-SiC with other fiber orientations (e.g. ± 45°) and the experimental verification will be conducted in our future work.

5. Conclusions

In this work, the effect of temperature on the material behavior of LSI based C/C-SiC was investigated and a modeling approach has been developed for the prediction of tensile properties at 1400 °C.

The main conclusions of this work are:

A complete material database of C/C-SiC was established with elastic constants, strength, fracture strain under various loadings, specific heat capacity as well as coefficient of thermal expansion and thermal conductivity in in-plane and out-of-plane directions. These values are the first design parameters, which enable the material-appropriate design of components made of C/C-SiC composite.

The influence of the temperature on the mechanical behavior was determined through tensile test conducted at RT, 1200 °C and 1400 °C. Since the Young's modulus remains constant in the whole range from RT to HT, the tensile strength increased slightly. Despite the large standard deviation, a decreasing tendency of the mean value of the fracture strain can be recognized with increasing temperature.

Based on the analyses of different CTE of fiber and matrix, a concept focusing on the change of RTS and cracks distribution of C/C-SiC under tensile loading at various temperatures was developed, which can explain the different material behavior of C/C-SiC at RT and HT close to the max manufacturing temperature. This concept has been confirmed through the temperature dependent test results and the analysis of fracture surface by SEM.

Based on the analysis of tensile hysteresis measurements at RT, a modeling approach with bilinear model has been developed in this work for the description of the material behavior of C/C-SiC at 1400 °C. The calculated values and stress-strain curve show a very close correlation to the test results.

The results in this work show that C/C-SiC material has excellent high-temperature tensile properties. In general, its possible application range extends well over 1400 °C, though the fracture strain reduced slightly, the Young's modulus remains constant and the strength value increases with HT.

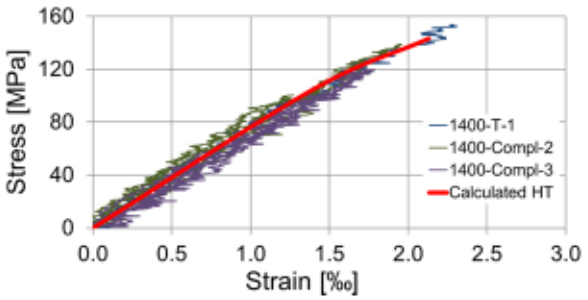

Fig. 14. Stress-strain comparison diagrams with test and calculated results for tensile investigation of C/C-SiC at 1400 °C.

Declaration of Competing Interest

The authors declare that they have no known competing financial interests or personal relationships that could have appeared to influence the work reported in this paper.

Acknowledgments

We want to thank Daniel Cepli and Raouf Jemmali at the DLR-Institute of Structures and Design and Jürgen Horvath at the Advanced Ceramics of University of Bremen for the collaboration and support for this work. This research did not receive any specific grant from funding agencies in the public, commercial, or not-for-profit sectors.

References

[1] R. Kochendörfer, N. Lützenburger, Applications of CMCs made via the liquid silicon infiltration (LSI) technique, in: W. Krenkel, R. Naslain, H. Schneider (Eds.), 4th International Conference on High Temperature Ceramic Matrix Composites (HT-CMC 4), Munich, Germany, 2001, pp. 277–287.

[2] W. Krenkel, B. Heidenreich, R. Renz, C/C-SiC composites for advanced friction systems, Adv. Eng. Mater. 4 (7) (2002) 427–436.

[3] W. Krenkel, F. Berndt, C/C–SiC composites for space applications and advanced friction systems, Mater. Sci. Eng. A 412 (1-2) (2005) 177–181.

[4] M. Frieß, R. Kochendörfer, R. Brandt, G. Neuer, H.-P. Maier, W. Krenkel, Ceramic matrix composites : the key materials for Re-entry from space to earth, in: D. Jacob, G. Sachs, S. Wagner (Eds.), Basic Research and Technologies for Two-Stage-to Orbit Vehicles, Wiley-VCH, Weinheim, Germany, 2005, pp. 499–526.

[5] B. Heidenreich, Manufacture and applications of C/C-SiC and C/SiC composites, in: J.P. Singh, N.P. Bansal, T. Goto, J. Lamon, S.R. Choi, M.M. Mahmoud, G. Link (Eds.), Processing and Properties of Advanced Ceramics and Composites IV, 2012, pp. 183–198.

[6] F. Breede, S. Hofmann, N. Jain, R. Jemmali, Design, manufacture, and characterization of a carbon fiber-reinforced silicon carbide nozzle extension, Int. J. Appl. Ceram. Technol. 13 (1) (2016) 3–16.

[7] W. Ding, Y. Shi, F. Kessel, D. Koch, T. Bauer, Characterization of corrosion resistance of C/C–SiC composite in molten chloride mixture MgCl2/NaCl/KCl at 700 °C, Npj Mater. Degrad. 3 (1) (2019).

[8] V. Stahl, Y. Shi, W. Kraft, T. Lanz, P. Vetter, R. Jemmali, F. Kessel, D. Koch, C/C-SiC component for metallic phase change materials, Int. J. Appl. Ceram. Technol. 17 (5) (2020) 2040–2050.

[9] Y. Shi, S. Hönig, M. Frieß, D. Koch, Manufacture and characterization of all-oxide ceramic matrix composites based on pre-impregnated fabrics, in: 6th International Congress on Ceramics, Dresden, Germany, 2016.

[10] E. Volkmann, K. Tushtev, D. Koch, C. Wilhelmi, J. Göring, K. Rezwan, Assessment of three oxide/oxide ceramic matrix composites: mechanical performance and effects of heat treatments, Compos. Part A Appl. Sci. Manuf. 68 (2015) 19–28.

[11] X. Cao, X. Yin, X. Fan, K. Zhao, H. Luo, L. Cheng, L. Zhang, High-temperature flexural properties of SiBC modified C/SiC composites, Ceram. Int. 40 (4) (2014) 6185–6190.

[12] C.P. Yang, L. Zhang, B. Wang, T. Huang, G.Q. Jiao, Tensile behavior of 2D-C/SiC composites at elevated temperatures: experiment and modeling, J. Eur. Ceram. Soc. 37 (4) (2017) 1281–1290.

[13] D.H. Yoon, J.W. Lee, J.H. Kim, I.C. Sihn, B.J. Lim, Fracture behavior of C/SiC composites at elevated temperature, J. Mech. Sci. Technol. 31 (8) (2017) 3647–3651.

[14] M. Patel, M.P.S. Kiran, S. Kumari, V. Singh, S. Singh, V.V.B. Prasad, Effect of oxidation and residual stress on mechanical properties of SiC seal coated C/SiC composite, Ceram. Int. 44 (2) (2018) 1633–1640.

[15] F. Su, P. Huang, Microscopic mechanism of the high-temperature strength behaviour of a C/SiC composite, Appl. Compos. Mater. 26 (3) (2019) 1059–1071.

[16] T. Cheng, R. Zhang, Y. Pei, S. Ai, R. He, Y. Zhao, D. Fang, Y. Yang, Tensile properties of two-dimensional carbon fiber reinforced silicon carbide composites at temperatures up to 1800 C in air, Extreme Mech. Lett. 31 (2019), 100546.
[17] T. Cheng, X. Wang, R. Zhang, Y. Pei, S. Ai, R. He, D. Fang, Y. Yang, Tensile properties of two-dimensional carbon fiber reinforced silicon carbide composites at temperatures up to 2300 C, J. Eur. Ceram. Soc. 40 (3) (2020) 630 635.
[18] C.C. Evans, A.C. Parmee, R.W. Rainbow, Silicon treatment of carbon fiber-carbon composites, in: 4th London Conference on Carbon and Graphite Society of Chemical Industry, London, 1974, pp. 231 235.
[19] W. Krenkel, Entwicklung eines kostengünstigen Verfahrens zur Herstellung von Bauteilen aus keramischen Verbundwerkstoffen, University of Stuttgart, Cologne, Germany, 2000, p. 214.
[20] B. Heidenreich, S. Hofmann, R. Jemmali, M. Frie , D. Koch, C/C-SiC materials based on melt infiltration - manufacturing methods and experiences from serial production, The Eighth International Conference on High Temperature Ceramic Matrix Composites (HTCMC 8) (2013).
[21] S. Hofmann, B. Öztürk, D. Koch, H. Voggenreiter, Experimental and numerical evaluation of bending and tensile behaviour of carbon-fibre reinforced SiC, Compos. Part A Appl. Sci. Manuf. 43 (11) (2012) 1877 1885.
[22] F. Breede, D. Koch, E. Maillet, G.N. Morscher, Modal acoustic emission of damage accumulation in C/C SiC composites with different fiber architectures, Ceram. Int. 41 (9, Part B) (2015) 12087 12098.
[23] Y. Shi, Y. Xiu, D. Koch, Investigation of statistical distribution of C/C-SiC composite s mechanical properties, Key Eng. Mater. 809 (2019) 131 139.
[24] E. Vagaggini, J.-M. Domergue, A.G. Evans, Relationships between hysteresis measurements and the constituent properties of ceramic matrix composites: I, theory, J. Am. Ceram. Soc. 78 (10) (1995) 2709 2720.
[25] J.-M. Domergue, E. Vagaggini, A.G. Evans, Relationships between hysteresis measurements and the constituent properties of ceramic matrix composites: II, experimental studies on unidirectional materials, J. Am. Ceram. Soc. 78 (10) (1995) 2721 2731.
[26] K.G. Dassios, D.G. Aggelis, E.Z. Kordatos, T.E. Matikas, Cyclic loading of a SiC-fiber reinforced ceramic matrix composite reveals damage mechanisms and thermal residual stress state, Compos. Part A Appl. Sci. Manuf. 44 (2013) 105 113.
[27] K.G. Dassios, T.E. Matikas, Residual stress-related common intersection points in the mechanical behavior of ceramic matrix composites undergoing cyclic loading, Exp. Mech. 53 (6) (2013) 1033 1038.
[28] Y. Deng, W. Li, X. Wang, H. Kou, X. Zhang, J. Shao, Y. Li, X. Zhang, J. Ma, Y. Tao, L. Chen, Temperature-dependent tensile strength model for 2D woven fiber reinforced ceramic matrix composites, J. Am. Ceram. Soc. 101 (11) (2018) 5157 5165.
[29] L. Li, Temperature-dependent proportional limit stress of SiC/SiC fiber-reinforced ceramic-matrix composites, High Temp. Mater. Process. 39 (1) (2020) 209.
[30] J. Schulte-Fischedick, S. Seiz, N. Lützenburger, A. Wanner, H. Voggenreiter, The crack development on the micro- and mesoscopic scale during the pyrolysis of carbon fibre reinforced plastics to carbon/carbon composites, Compos. Part A Appl. Sci. Manuf. 38 (10) (2007) 2171 2181.
[31] N. Jain, M. Kosin, Y. Shi, D. Koch, Characterization and modeling of transverse micro-cracking during pyrolysis process of carbon fiber reinforced plastics, Int. J. Appl. Ceram. Technol. 0 (0) (2019).
[32] F.H. Gern, R. Kochendörfer, Liquid silicon infiltration: description of infiltration dynamics and silicon carbide formation, Compos. Part A Appl. Sci. Manuf. 28 (4) (1997) 355 364.
[33] DIN EN, 1389: Advanced Technical Ceramics - Ceramic Composites - Physical Properties - Determination of Density and Apparent Porosity, 2004.
[34] W.J. Parker, R.J. Jenkins, C.P. Butler, G.L. Abbott, Flash method of determining thermal diffusivity, heat capacity, and thermal conductivity, J. Appl. Phys. 32 (9) (1961) 1679 1684.
[35] C. Pradere, C. Sauder, Transverse and longitudinal coefficient of thermal expansion of carbon fibers at high temperatures (300 2500K), Carbon 46 (14) (2008) 1874 1884.
[36] D.N. Talwar, J.C. Sherbondy, Thermal expansion coefficient of 3C SiC, Appl. Phys. Lett. 67 (22) (1995) 3301 3303.
[37] Y. Shi, A. Neubrand, D. Koch, Characterization of hardness and stiffness of ceramic matrix composites through instrumented indentation test, Adv. Eng. Mater. 21 (5) (2018), 1800806.
[38] T. Tenax®, Fiber Data - HTA, http://www.tohotenax.com/tenax/en/products/st_property.php. Version: 2009.
[39] S. Weber, Entwicklung und Herstellung von MiCaSiC® - Keramiken über die Flüssigphaseninfiltration von komplexen und neuartigen Kohlenstoffstrukturen, University Stuttgart, Stuttgart, Germany, 2016.
[40] P. Galizia, L. Zoli, D. Sciti, Impact of residual stress on thermal damage accumulation, and Young s modulus of fiber-reinforced ultra-high temperature ceramics, Mater. Des. 160 (2018) 803 809.
[41] M. Steen, Anomalous stress-strain behaviour of CFCCs: an extreme form of scatter, Adv. Compos. Mater. 8 (1) (1999) 127 134.
[42] M. Steen, Tensile mastercurve of ceramic matrix composites: significance and implications for modelling, Mater. Sci. Eng. A 250 (2) (1998) 241 248.